Supplementary figure titles and legends

Figure S1 (related to Fig 1). RAMP2 purification and effects on GCGR-induced G_s turnover.

(**A**) Schematic of the RAMP2 growth and purification protocol, size exclusion chromatography profile demonstrating purity, as well as stability to repeated size exclusion runs. (**B**) Time-dependent GTP turnover assay demonstrating GDP-independent turnover for G_s alone and

enhancement in turnover in the presence of agonist-bound GCGR. Addition of RAMP2 results in a [GDP] dependent inhibition in this turnover rate even past G_s alone. (**C**) GTP turnover assay demonstrating that RAMP2 inhibition is specific to GCGR and not observed for β_2AR. (**D**) GTP turnover assay demonstrating that while RAMP2 has no direct effects on β_2AR turnover, GCGR/RAMP2 complex is able to sequester away G_s from and inhibit β_2AR dependent turnover. P values in **C** and **D** are denoted as follows: ns ($P>0.05$), * ($P\leq0.05$), ** ($P\leq0.01$), *** ($P\leq0.001$), and **** ($P\leq0.0001$). (**E**) Individual example BRET affinity experiments demonstrating changes in affinity and total change in BRET in the absence and presence of RAMP2 for the three TAMRA-labeled glucagon analogues used here.

Figure S2 (related to Fig 2). Characterizing ZP7680 and RAMP2 effects on GRK phosphorylation of GCGR.
Schild plots were generated for the antagonist des-His1[Glu9]-Glucagon-amide (**A**) and ZP7680 (**B**) in the absence of IBMX and indicated that ZP7680 is effective in blocking the glucagon response at lower concentrations compared to des-His1[Glu9]-Glucagon-amide, which is reflected in a higher estimated affinity (K_B/pA2) from a Schild plot analysis (Fig. 2A). Data in **A** and **B** are representative curves from one experiment performed in duplicate from a total of 4 independent experiments of each. (**C**) Schematic depicting ATP depletion assay for kinase activity. (**D**) ATP depletion assay showing inhibition of GRK phosphorylation of GCGR in the presence of RAMP2. (**E**) Phosphorylation ProQ gels showing inhibition of GRK5 phosphorylation of GCGR by RAMP2 but (**F**) no inhibition of GCGR phosphorylation by GRK2.

Figure S3 (related to Fig 3). Perturbation in GCGR dynamics by RAMP2 observed by HX-MS.
(**A**) Effect of binding partner addition on deuterium uptake for RAMP2 (+/- GCGR, left) and GCGR (+/- RAMP2, right). Replicate experiments are shown as separate panels. The difference in the percent deuteration for a given peptide at a given time point is plotted against the sequence position. Brown peptides show less than a 5% difference in exchange between conditions, cyan peptides in RAMP2 are protected upon complexing with GCGR, and peptides that display unimodal and bimodal deprotection upon binding of RAMP2 are plotted in salmon and purple, respectively. (**B**) Replicate data for individual spectra of select peptides within regions of GCGR that display non-EX2 behavior as plotted in Fig. 2. (**C**) FLAG pulldown on RAMP2 assessed by SDS-PAGE gel demonstrating that antagonist peptide (ZP7680) bound GCGR interacts best with RAMP2.

Figure S4 (related to Fig 4). Site-specific labeling of mC-GCGR with cysteine-reactive groups and smFRET experiments.
(**A**) Schematic highlighting the reaction scheme used to block labile, off-target disulfides and allow for specific labeling at introduced cysteines on GCGR. The highly cysteine-reactive nitroxide spin label Proxyl was used to test for off-target labeling by observing with cwEPR. Briefly, introduced cysteines are labeled specifically with the nitroxide spin label RSSR, followed by iodoacetamide capping of residual free thiols, presumably selectively at labile disulfides. Finally, RSSR is stripped off with TCEP, allowing for subsequent labeling with highly reactive fluorophores or spin labels of interest. (**B**) smFRET distributions of cysteine labeled GCGR comparing antagonist (green, N=235) or antagonist and RAMP2 bound receptor (orange, N=176). (**C**) Example smFRET traces showing donor (green), acceptor (red) intensity values as well as the calculated FRET values (blue) for a series of ligand conditions including apo, antagonist, agonist, agonist and G_s, and agonist with G_s and RAMP2.

Figure S5 (related to Fig 5). Cryo-EM sample preparation and data processing.
Schematic depicting purification protocols (**A**) and complex formation (**B**). (**C**) Size exclusion chromatograms and SDS-PAGE gels demonstrating complex formation with RAMP2. (**D**) Cryo-EM data collection and processing pipeline, showing representative cryo-EM image of the GCGR-G_s-RAMP2 complex, reference-free 2D cryo-EM averages, and cryo-EM data processing flow chart, including particle selection, classifications, density map reconstructions, and the "gold standard" FSC curves from cryoSPARC. (**E**) Cryo-EM density map and model are shown for the seven transmembrane helices and ZP3780.

Figure S6 (related to Fig 5 and Fig 6). Broken ECD and agonist contacts in the presence of RAMP2 and 3D variability analysis.
In the presence of RAMP2, there is no structured density for a conserved disulfide between C43 and C67 in the ECD (**A**), as well as a loss of a hydrogen bond between K37 in the ECD and S213 in ECL1 along with a cation-pi interaction within the N-terminal helix of the ECD (**B**). Ligand contacts with TM1 and TM2 are also lost, as seen in the loss of contact between E20 in the agonist and Q131 in TM1 (**C**) and D195 in TM2 switching hydrogen bond partners from Q3 in the agonist to R199 within TM2 (**D**). (**E**) The first (red) and last (light blue) frames within each of the 3 major principal components of the 3D variability analysis implemented in cryoSPARC. (**F**) Covalently crosslinked GCGR-RAMP2-G_s was subjected to cryo-EM imaging. The resulting particles were low-resolution, and only contained structured density for GCGR/RAMP2 or GCGR/G_s containing particles (not shown). The 2D reference-free class averages show density that corresponds well to the orientation predicted from AlphaFold for the GCGR/RAMP2 interface, i.e. both in an "upwards" conformation.

Figure S7 (related to Fig 5). Differences in ECD conformation between glucagon-family and calcitonin-family Family B GPCRs.
The structures of calcitonin-like receptor (CLR) bound to each of RAMP1 (CGRP, **A**), RAMP2 (AM1, **B**), or RAMP3 (AM2, **C**) display slight differences in binding pose but broadly bind to the CLR ECD with the N-terminal helix in an orientation near perpendicular to the bilayer norm. In contrast, the peptide-bound GCGR ECD is in an orientation that is incompatible with the same binding pose as that observed for CLR (**D**), even though there is some flexibility in this region in glucagon receptor family members (**E**).

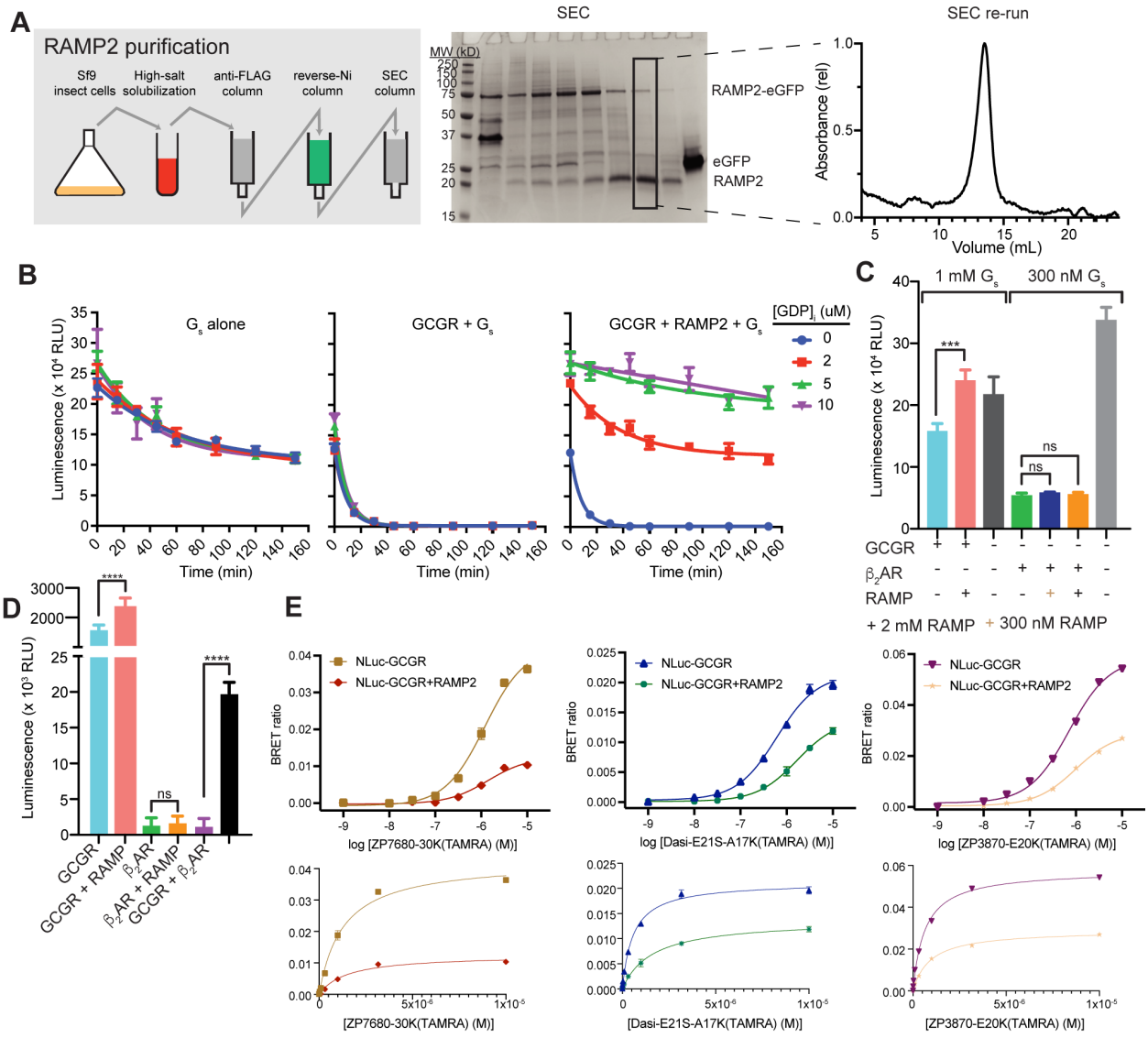
A
RAMP2 purification
Sf9 insect cells
High-salt solubilization
anti-FLAG column
reverse-Ni column
SEC column
SEC
MW (kD)
RAMP2-eGFP
eGFP
RAMP2
SEC re-run
Absorbance (rel)
Volume (mL)
B
Gs alone
GCGR + Gs
GCGR + RAMP2 + Gs
[GDP]i (uM)
Luminescence (x 10⁴ RLU)
Time (min)
C
1 mM Gs
300 nM Gs
GCGR
β2AR
RAMP
+ 2 mM RAMP
+ 300 nM RAMP
D
Luminescence (x 10³ RLU)
GCGR
GCGR + RAMP
β2AR
β2AR + RAMP
GCGR + β2AR
E
NLuc-GCGR
NLuc-GCGR+RAMP2
BRET ratio
log [ZP7680-30K(TAMRA) (M)]
log [Dasi-E21S-A17K(TAMRA) (M)]
log [ZP3870-E20K(TAMRA) (M)]
[ZP7680-30K(TAMRA) (M)]
[Dasi-E21S-A17K(TAMRA) (M)]
[ZP3870-E20K(TAMRA) (M)]

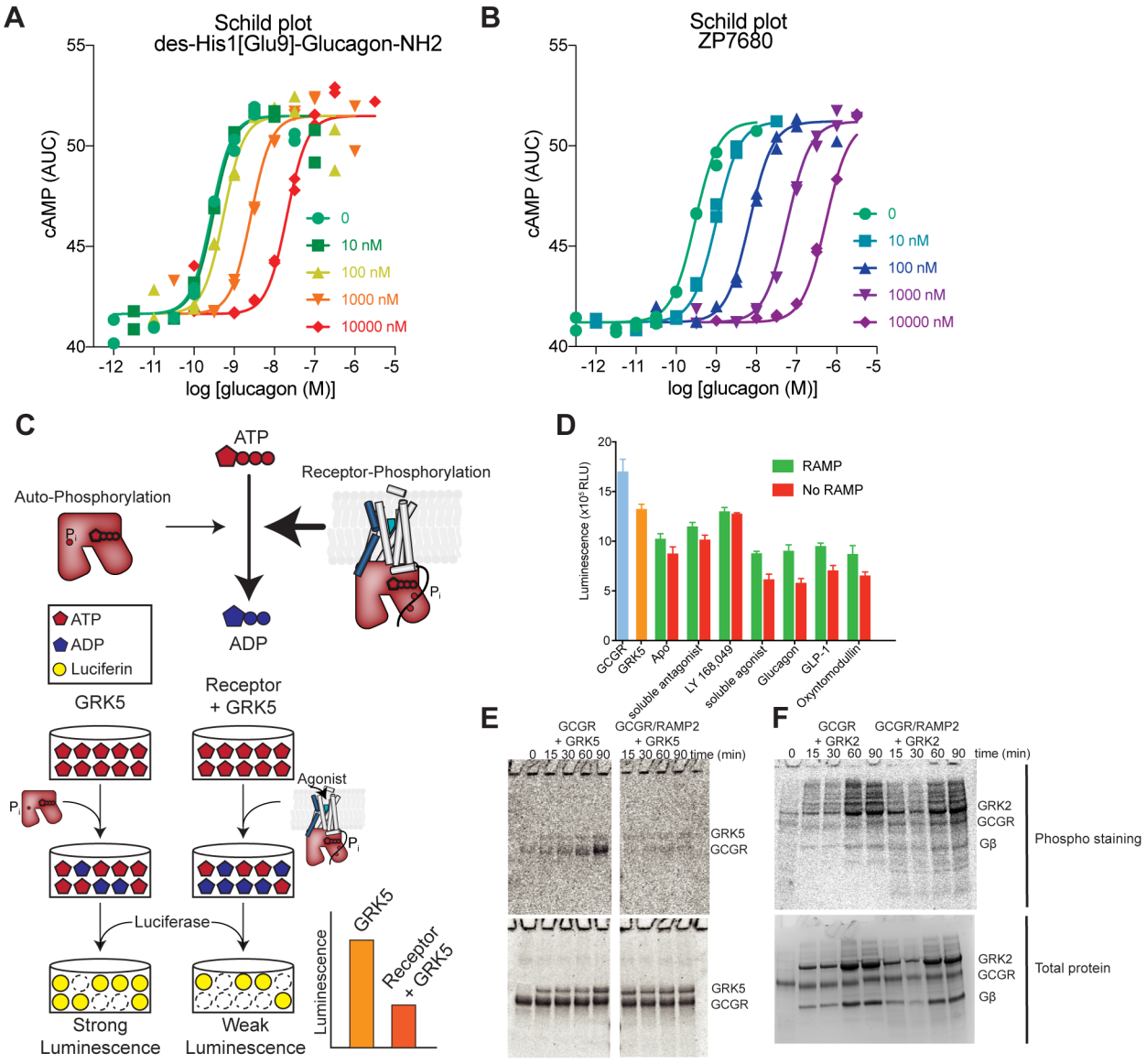
A
Schild plot
des-His1[Glu9]-Glucagon-NH2
cAMP (AUC)
log [glucagon (M)]
0
10 nM
100 nM
1000 nM
10000 nM
B
Schild plot
ZP7680
cAMP (AUC)
log [glucagon (M)]
0
10 nM
100 nM
1000 nM
10000 nM
C
ATP
Auto-Phosphorylation
Receptor-Phosphorylation
ADP
ATP
ADP
Luciferin
GRK5
Receptor
+ GRK5
Agonist
Luciferase
Strong
Luminescence
Weak
Luminescence
Luminescence
GRK5
Receptor
+ GRK5
D
Luminescence (x10⁶ RLU)
RAMP
No RAMP
GCGR
GRK5
Apo
solubie antagonist
LY 168,049
soluble agonist
Glucagon
GLP-1
Oxyntomodulin
E
GCGR
+ GRK5
GCGR/RAMP2
+ GRK5
0 15 30 60 90 15 30 60 90 time (min)
GRK5
GCGR
GRK5
GCGR
F
GCGR
+ GRK2
GCGR/RAMP2
+ GRK2
0 15 30 60 90 15 30 60 90 time (min)
GRK2
GCGR
Gβ
Phospho staining
GRK2
GCGR
Gβ
Total protein

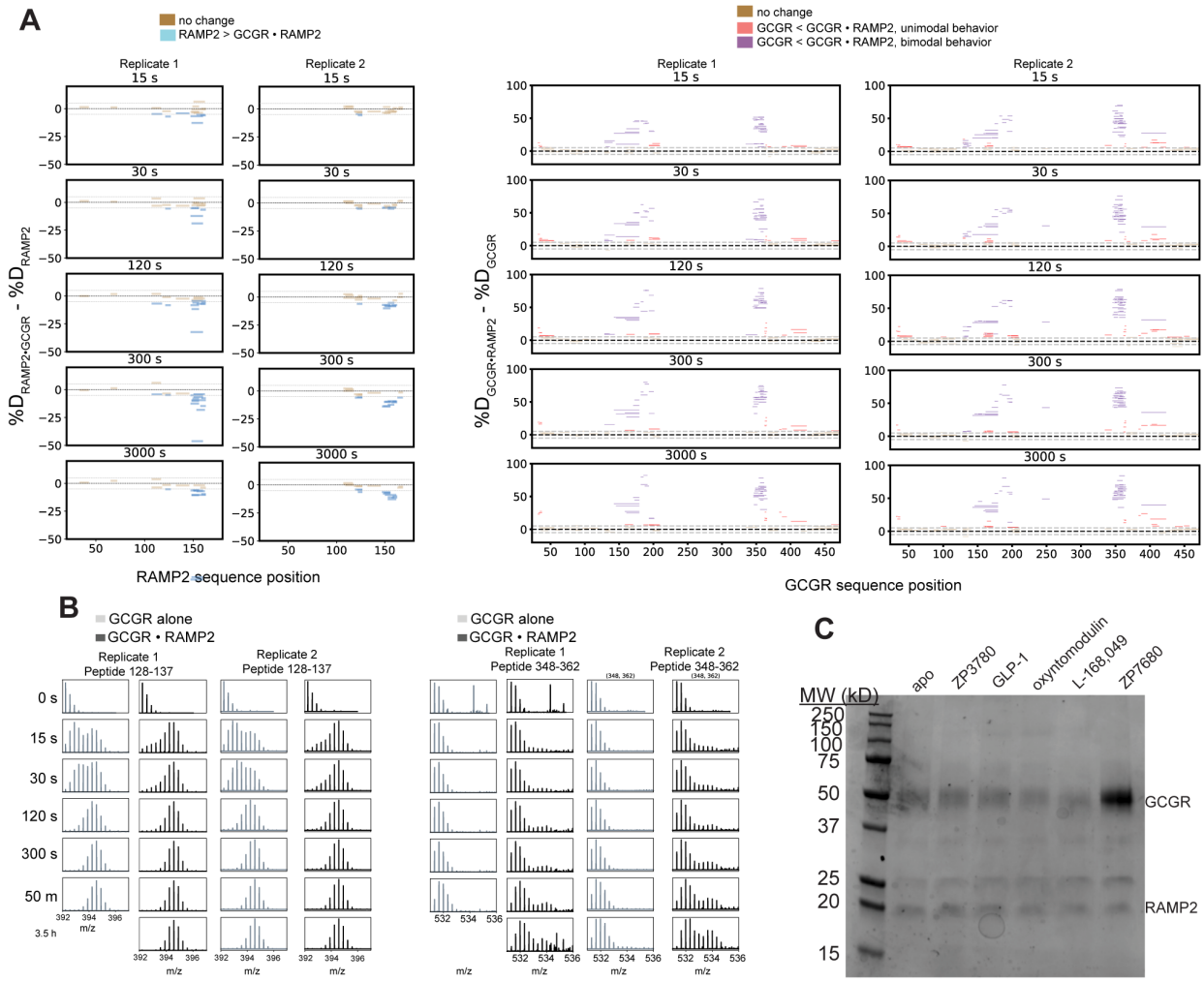
A
no change
RAMP2 > GCGR • RAMP2
Replicate 1
Replicate 2
15 s
30 s
120 s
300 s
3000 s
%D RAMP2•GCGR - %D RAMP2
RAMP2 sequence position
no change
GCGR < GCGR • RAMP2, unimodal behavior
GCGR < GCGR • RAMP2, bimodal behavior
%D GCGR•RAMP2 - %D GCGR
GCGR sequence position
B
GCGR alone
GCGR • RAMP2
Peptide 128-137
Peptide 348-362
0 s
15 s
30 s
120 s
300 s
50 m
3.5 h
m/z
C
MW (kD)
apo
ZP3780
GLP-1
oxyntomodulin
L-168,049
ZP7680
250
150
100
75
50
37
25
20
15
GCGR
RAMP2

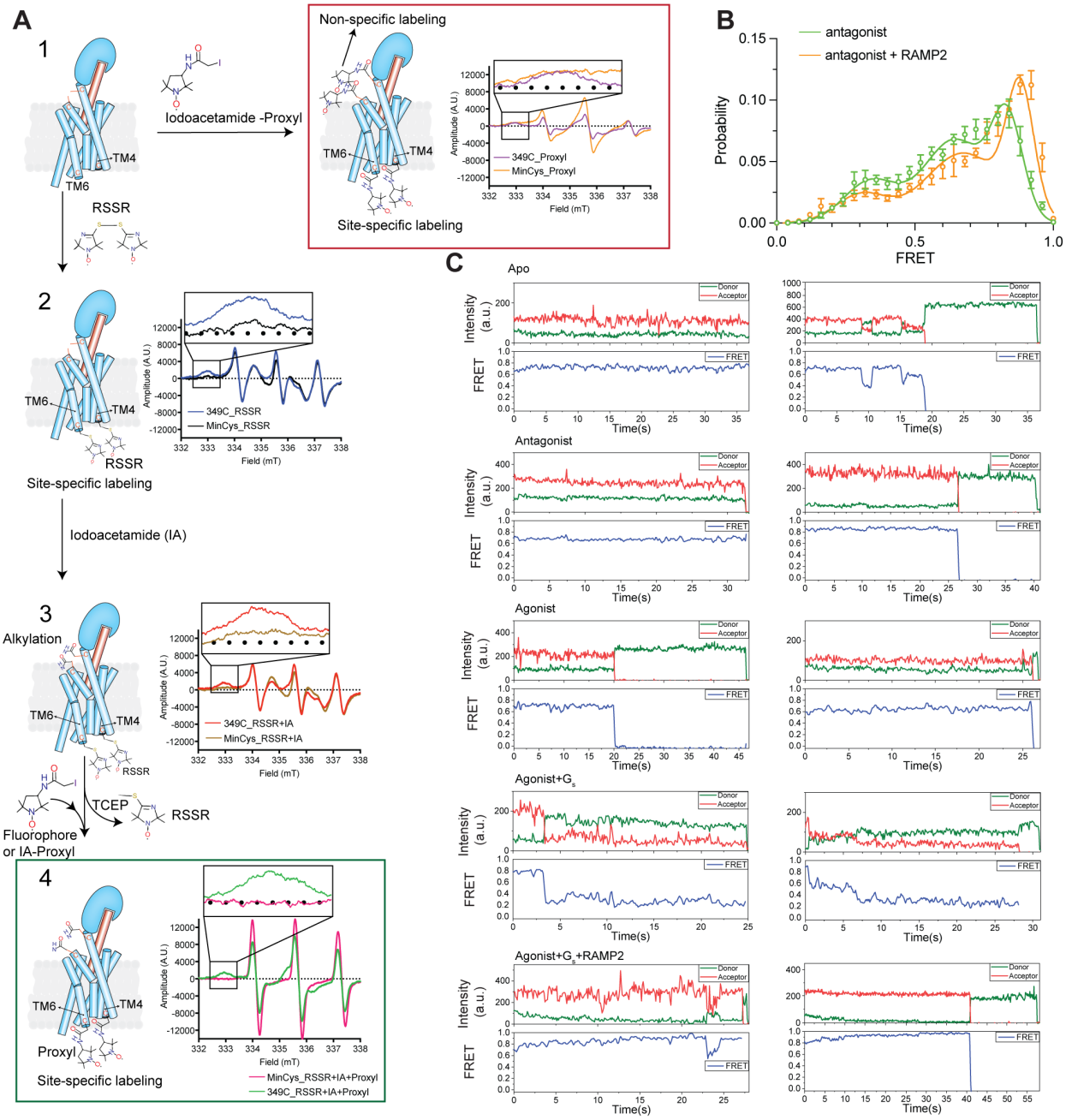
A
1
Iodoacetamide -Proxyl
TM6
TM4
RSSR
Non-specific labeling
Site-specific labeling
349C_Proxyl
MinCys_Proxyl
Amplitude (A.U.)
Field (mT)
2
349C_RSSR
MinCys_RSSR
Site-specific labeling
Iodoacetamide (IA)
3
Alkylation
349C_RSSR+IA
MinCys_RSSR+IA
TCEP
Fluorophore
or IA-Proxyl
4
Proxyl
MinCys_RSSR+IA+Proxyl
349C_RSSR+IA+Proxyl
B
antagonist
antagonist + RAMP2
Probability
FRET
C
Apo
Antagonist
Agonist
Agonist+G$_s$
Agonist+G$_s$+RAMP2
Donor
Acceptor
Intensity (a.u.)
FRET
Time(s)

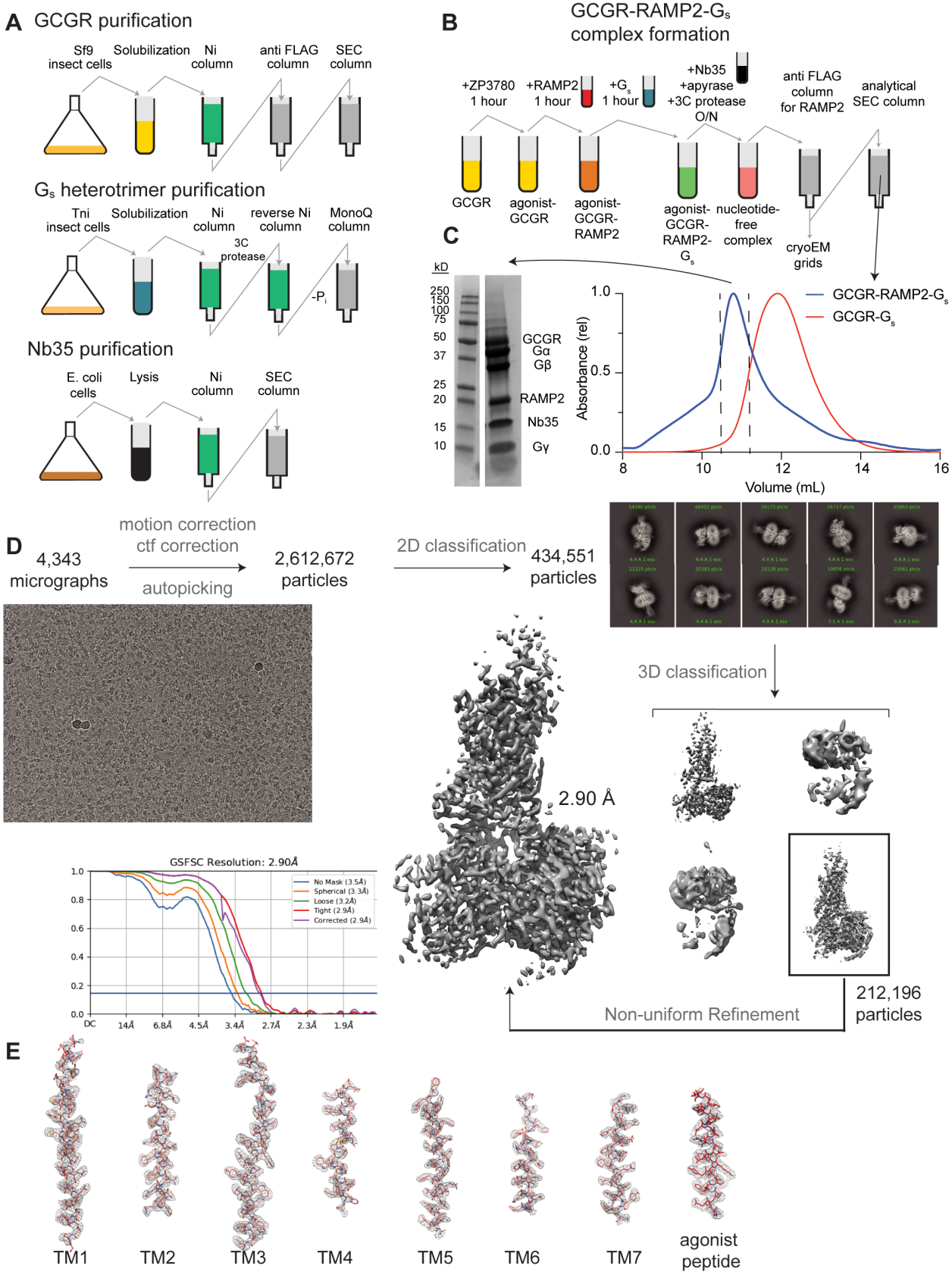
A GCGR purification
Sf9 insect cells
Solubilization
Ni column
anti FLAG column
SEC column
Gs heterotrimer purification
Tni insect cells
Solubilization
Ni column
3C protease
reverse Ni column
MonoQ column
-Pi
Nb35 purification
E. coli cells
Lysis
Ni column
SEC column
B GCGR-RAMP2-Gs complex formation
+ZP3780 1 hour
+RAMP2 1 hour
+Gs 1 hour
+Nb35 +apyrase +3C protease O/N
anti FLAG column for RAMP2
analytical SEC column
GCGR
agonist-GCGR
agonist-GCGR-RAMP2
agonist-GCGR-RAMP2-Gs
nucleotide-free complex
cryoEM grids
C
kD
250
150
100
75
50
37
25
20
15
10
GCGR
Gα
Gβ
RAMP2
Nb35
Gγ
Absorbance (rel)
1.0
0.5
0.0
8
10
12
14
16
Volume (mL)
GCGR-RAMP2-Gs
GCGR-Gs
D
4,343 micrographs
motion correction
ctf correction
autopicking
2,612,672 particles
2D classification
434,551 particles
3D classification
2.90 Å
212,196 particles
Non-uniform Refinement
GSFSC Resolution: 2.90Å
No Mask (3.5Å)
Spherical (3.3Å)
Loose (3.2Å)
Tight (2.9Å)
Corrected (2.9Å)
1.0
0.8
0.6
0.4
0.2
0.0
DC
14Å
6.8Å
4.5Å
3.4Å
2.7Å
2.3Å
1.9Å
E
TM1
TM2
TM3
TM4
TM5
TM6
TM7
agonist peptide

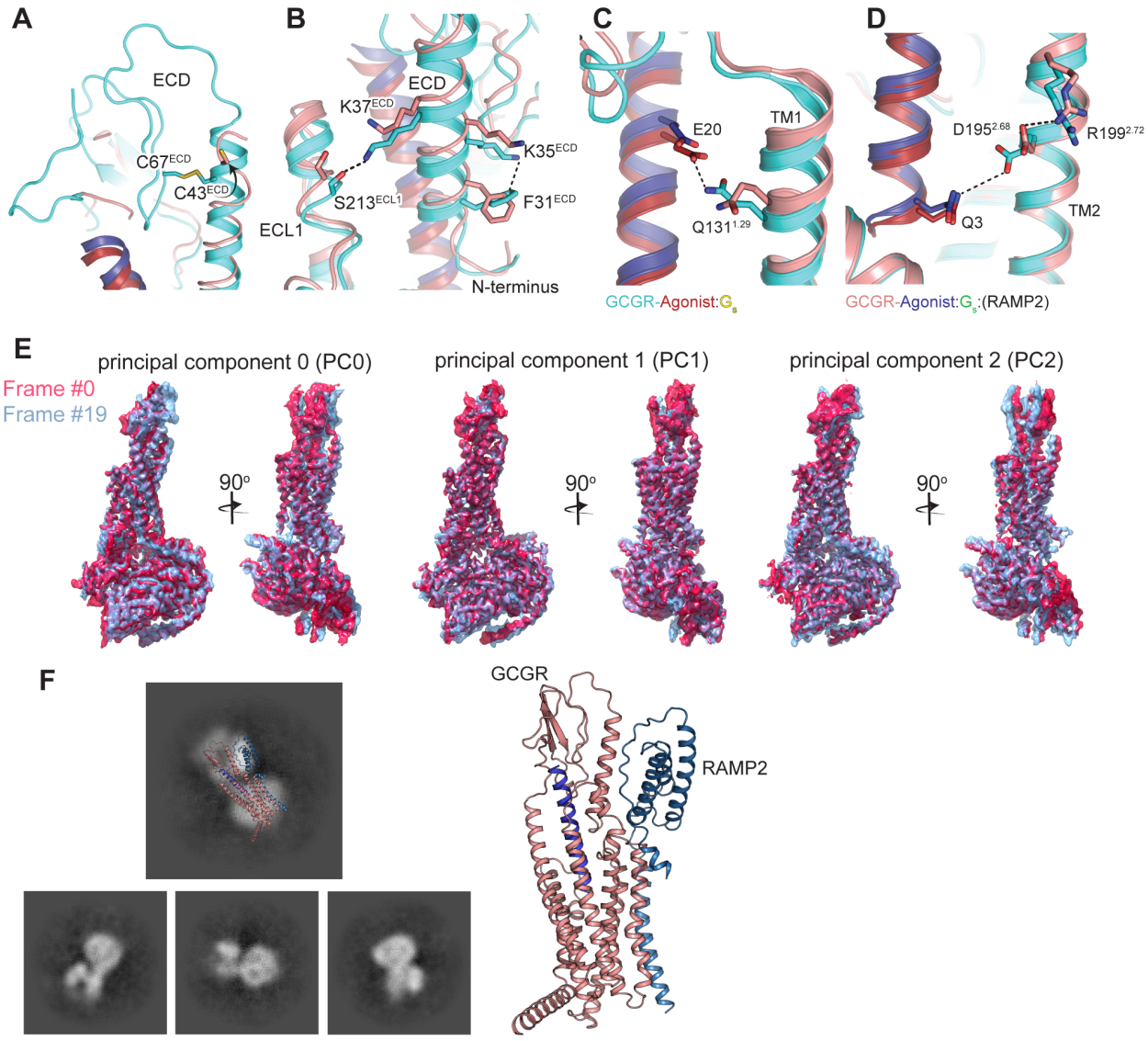
A
ECD
C67ECD
C43ECD
B
ECD
K37ECD
K35ECD
S213ECL1
F31ECD
ECL1
N-terminus
C
E20
TM1
Q1311.29
GCGR-Agonist:Gs
D
D1952.68
R1992.72
Q3
TM2
GCGR-Agonist:Gs:(RAMP2)
E
principal component 0 (PC0)
principal component 1 (PC1)
principal component 2 (PC2)
Frame #0
Frame #19
90°
90°
90°
F
GCGR
RAMP2

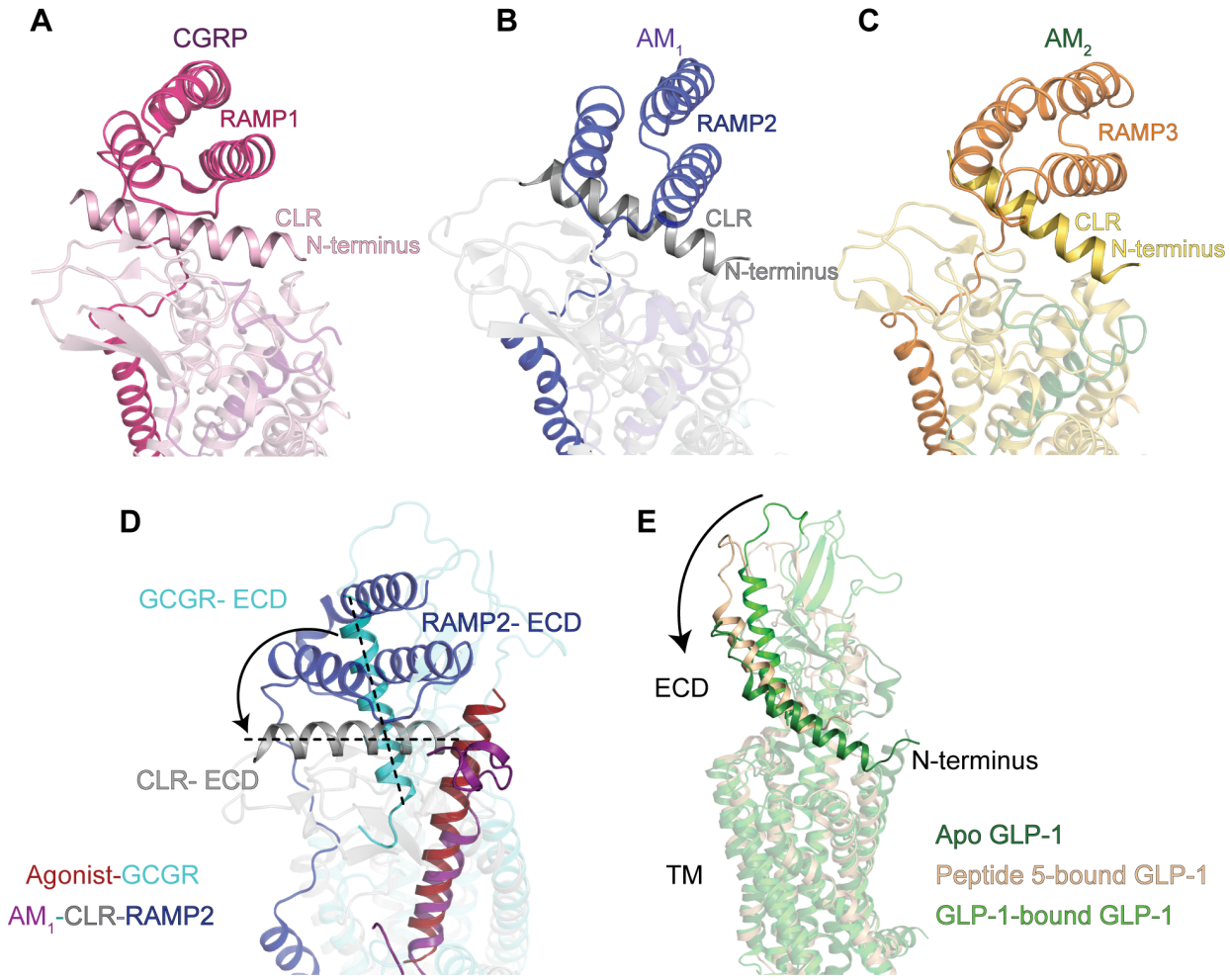
A
CGRP
RAMP1
CLR
N-terminus
B
AM1
RAMP2
CLR
N-terminus
C
AM2
RAMP3
CLR
N-terminus
D
GCGR- ECD
RAMP2- ECD
CLR- ECD
Agonist-GCGR
AM1-CLR-RAMP2
E
ECD
N-terminus
TM
Apo GLP-1
Peptide 5-bound GLP-1
GLP-1-bound GLP-1